Council on Tall Buildings and Urban Habitat Korea

International Journal of
High-Rise Buildings
www.ctbuh-korea.org/ijhrb/index.php

International Journal of High-Rise Buildings
December 2022, Vol 11, No 4, 277-286
https://doi.org/10.21022/IJHRB.2022.11.4.277

Fluctuating Wind Pressures on High Aspect Ratio Circular Cylinder

Keisuke Miura[1†] and Masahiro Matsui[2]

[1]*Tokyo Electric Power Services Co., LTD., Tokyo, Japan*
[2]*Tokyo Polytechnic University, Kanagawa, Japan*

Abstract In this study, The POD technique was applied to the fluctuating wind pressure of high aspect ratio circular cylinder to consider about its organizational structure, and considered about the characteristics of the fluctuating wind force obtained by synthesized the POD modes.

Keywords Chimney, Circular cylinder, Fluctuating Lift Force, Power spectrum density, POD

[†]Corresponding author:
Keisuke Miura
Tel: +81-3-6372-5429
Fax: +81-3-6372-5158
E-mail:
kmiura@tepsco.co.jp

1. Introduction

In Japan, many chimneys for thermal power plants over 100m high have been built. Such super-high chimneys have a more slender shape than normal structures, often having aspect ratios of 20 or more. In such cases, "tower-supported chimneys," in which the horizontal forces acting on the exhaust cylinder are supported by a truss-type steel tower, are often adopted in Japan.

Most thermal power plants owned by electric power companies are more than 30 years old, and most would normally have been rebuilt. However, due to the recent interest in environmental issues, thermal power plants are not being rebuilt, even though demand for electric power continues to increase. Hence, the lives of existing thermal power plants need to be extended. Chimneys are one of the important facilities for operating thermal power plants and those are also aging. It is important not only to design for maximum wind loads, but also to prevent damage due to cumulative loads.

Cylindrical structures such as chimneys are a problem because of periodic lift oscillations caused by alternating vortices in their wakes, so-called vortex-induced vibrations, but cases of that have also been reported even in tower-supported chimneys (Homma et al., 2003). Wind tunnel experiments are effective for investigating dynamic phenomena caused by wind loads. However, when building a scale model for wind tunnel experiments, there is the problem in modeling size, weight, stiffness and so on. For example, when modeling a 200 m high tower-supported chimney, the minimum size of the components that configure the truss steel tower is only about 200 mm in diameter, which is only 2 mm for a 1/100 scale model. In addition, the model height is 2 m, and there are not many wind tunnels that can handle a model of that size. Hence, it is important to develop a method for evaluating dynamic response by numerical analysis.

In this study, wind pressure experiments carried out using a cylindrical model in which is the exhaust cylinder of the tower-supported chimney, in which the aspect ratio of cylindrical model is 12 to 25. Furthermore, the proper orthogonal decomposition (hereafter POD) technique was applied to the fluctuating wind pressure distribution to consider about its organizational structure. In addition, the characteristics of the fluctuating wind force synthesized by POD modes is discussed.

2. Wind Pressure Experiment

Wind pressure experiments were carried out at the wind engineering center of Tokyo Polytechnic University. Figure 1 shows the wind pressure experimental models which are aspect ratios $H/D = 12$ to 25. The heights are $H = 600$ mm to 1250mm and the diameter is $D = 500$ mm, at a scale of 1/160. These heights of the model are 100m to 200 m in real scale. Twenty pressure taps were placed around the circumference in 10 locations in the vertical direction. Roughness was imparted to the model surface by 1 mm-square plastic bars to determine the influence of Reynolds number (Marukawa et al., 1984). In this experiment, the top of the model was fixed to the wind tunnel ceiling with a stainless steel wire to suppress its vibration.

The mean wind speed U_H at the model's top varied from 3 m/s to 17 m/s, and the Reynolds number varied from $R_e = 1.1 \times 10^4$ to 6.0×10^4. Figure 2 shows the wind profile of the wind pressure experiment. The power law is $a = 0.27$ (terrain type IV in AIJ, 2015), turbulence intensity is $Iu = 10\%$ at $H = 800$ mm ($= 2/3H$ of $H/D = 25$), and turbulence scale is $L \approx 0.46$ m, which is 74.3 m in real scale. The data sampling frequency of the wind

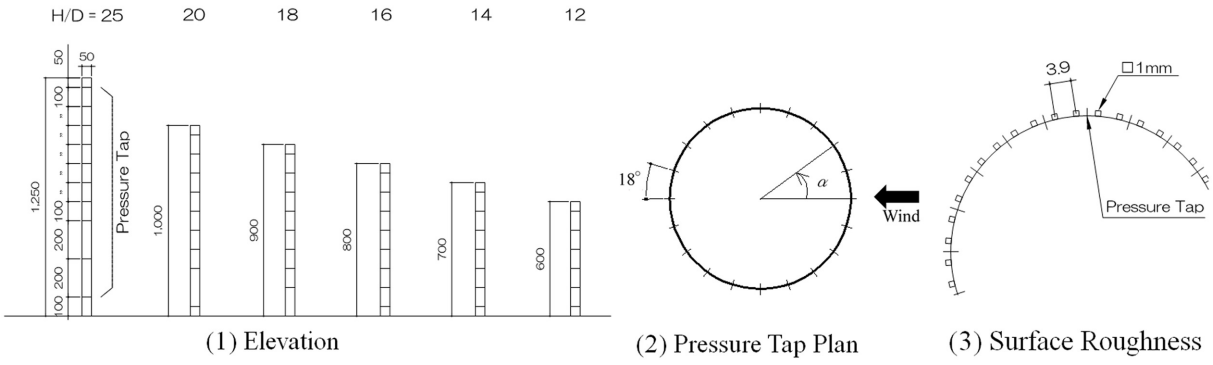


Figure 1. Wind pressure experimental models.

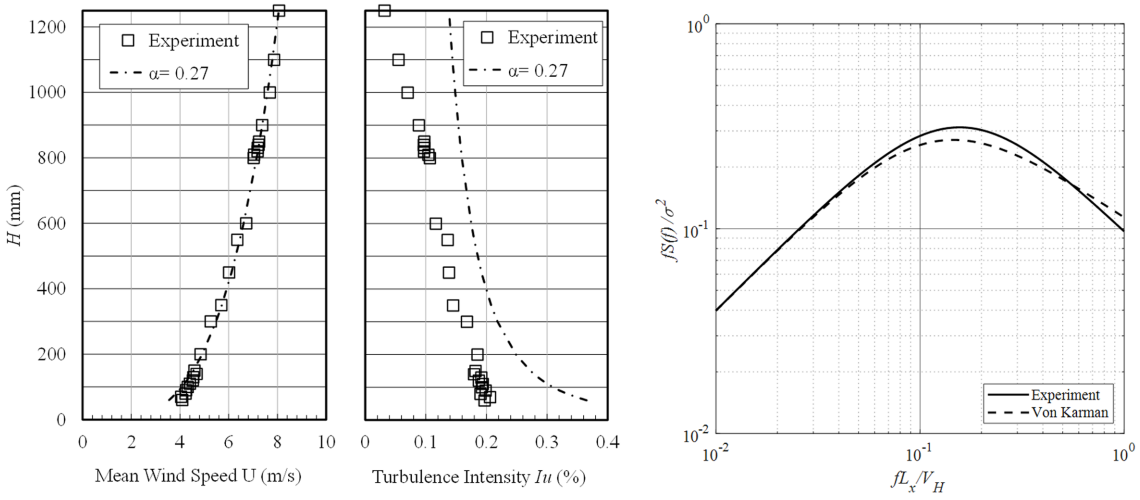


Figure 2. Wind profile and power spectrum density.

pressure experiment is 800 Hz, and the number of data acquired was 288,000.

3. Experiment Results

Figure 3 compares wind pressure coefficient $\overline{C_p}$ with previous result. Marukawa et al. (1984) measured wind pressures on a 200 m-high reinforced concrete chimney (in this case $H/D = 13.5$). Katagiri et al. (1986) carried out wind tunnel experiments on a wind pressure model of $H/D = 20$. The $\overline{C_p}$ results for the same aspect ratios are shown here as solid lines for comparison with results of previous experiments. The experimental results are in

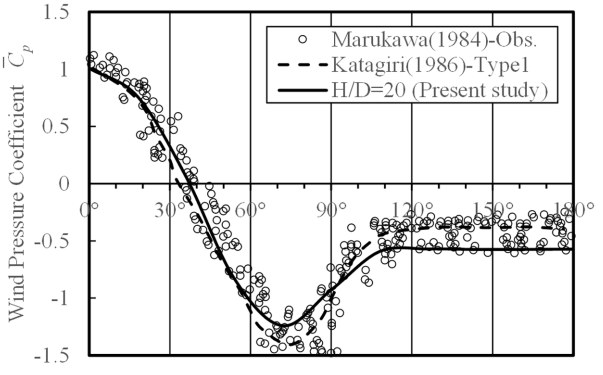


Figure 3. Comparison of mean wind pressure coefficient with previous results.

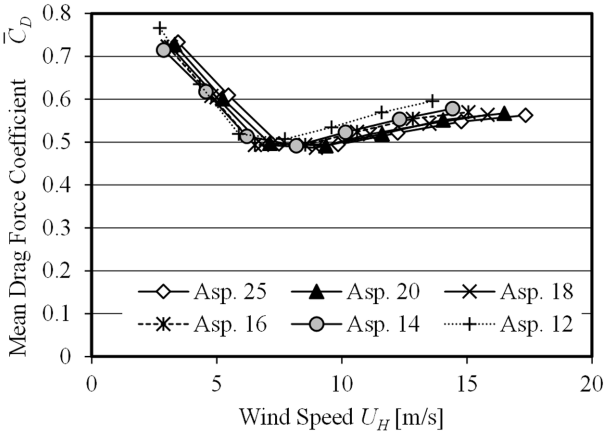


Figure 4. Variation of mean drag force coefficient with wind speed and aspect ratio.

general agreement with the full scale measurement results of Marukawa et al. (1984) and the wind tunnel experiment results of Katagiri et al. (1986). The inflection point at which the change in $\overline{C_p}$ becomes almost constant is found at $\theta = 100°\sim110°$, and it is considered to be the point of vortex shedding. These results correspond to those of Roshko (1961), which were obtained by simulating a transcritical Reynolds number region.

Figure 4 shows the variation of mean drag force coefficient $\overline{C_D}$ with U_H and H/D. $\overline{C_D}$ is defined by the following equations.

$$\overline{C_D} = \frac{\overline{F_D}}{q_H A} \tag{1}$$

$$\overline{F_D} = \int_H \int_\theta \overline{C_p} \sin\theta d\theta dz \tag{2}$$

where q_H is velocity pressure, A is model area ($= D \times H$), *and 6* is pressure tap point angle relative to wind direction. The result of $\overline{C_D}$ was simulated the phenomenon in which the periodicity of the wake vortex disappears as it changes from the subcritical to the supercritical region, and in which the periodicity of the wake vortex recovers as it changes from the supercritical to the transcritical region. Hereafter, in this study discuss the results for $U_H = 15\sim17$ m/s, which the periodicity of the wake vortex is considered to have recovered.

Figure 5 shows the contour lines of the mean wind pressure coefficient $\overline{C_p}$ for H/D = 12, 16, 20, and 25. The ordinate is normalized by height H. As shown in Figure 3, $\overline{C_p}$ is constant above the wind pressure measurement point $\theta = 100°$, but the height range varies depending on the aspect ratio.

For example, for H/D=12, the pressure is constant in the range of $z/H = 0.2\sim0.8$, while for $H/D = 25$, the pressure varies from $z/H = 0.4\sim0.9$, indicating that the range in which the vortex shedding is two-dimensional varies with aspect ratio. Furthermore, the influence range of the three-dimensional vortex shedding from the free edge also depends on the aspect ratio, ranging from $z/H = 0.8\sim1.0$ for H/D = 12, but localized to $z/H = 0.9\sim1.0$ for $H/D = 25$.

Figure 6 shows the contour line of the fluctuating wind pressure coefficient C_p' for H/D = 12, 16, 20, and 25. The distribution of C_p' decreases as the aspect ratio increases. This is thought to indicate the effect of the wind profile's turbulence intensity. For all aspect ratios, there is a local increase in C_p' near the model's free edge at $\theta = 90$, and a similar trend is observed at $z/H = 0.4$. On the other hand, C_p' decreases for $\theta = 180$, $z/H = 0.6\sim0.8$. This is considered because alternating wake vortex interfere with each other

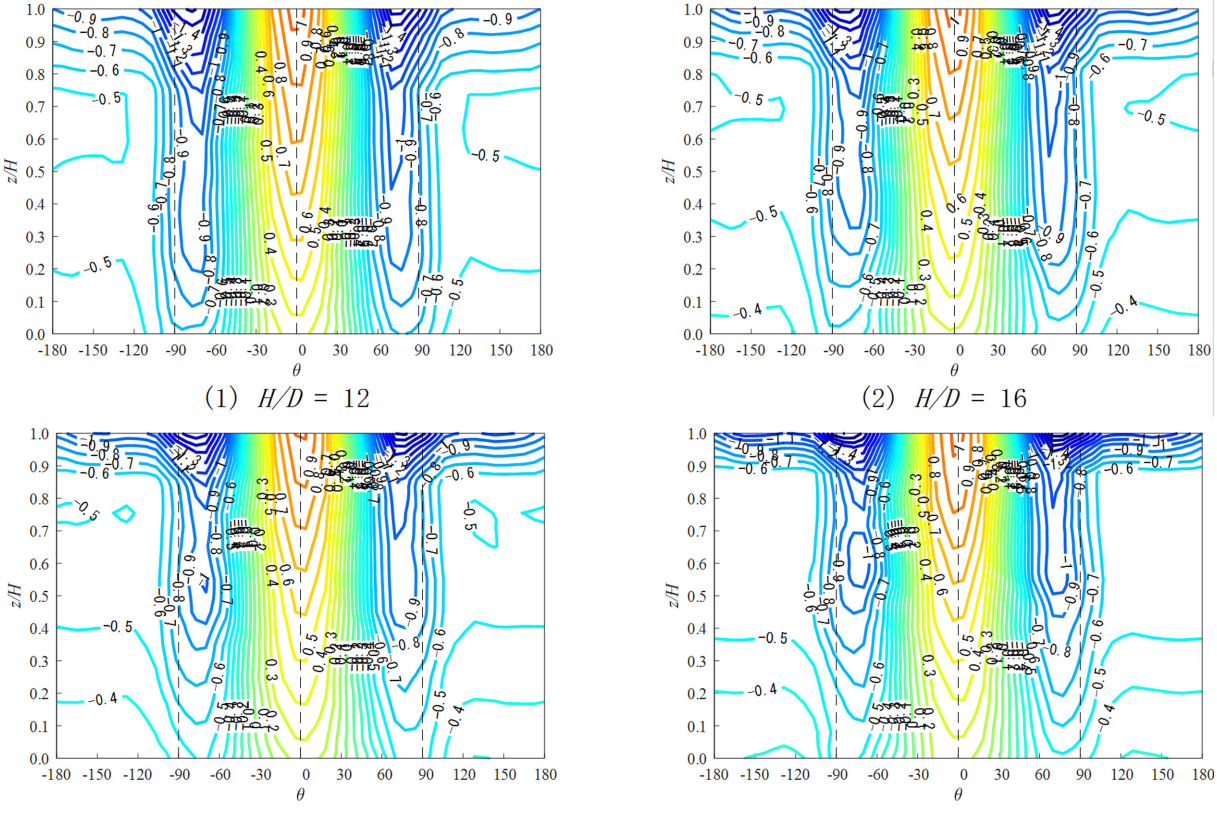


Figure 5. Comparison of mean wind pressure coefficient with aspect ratio.

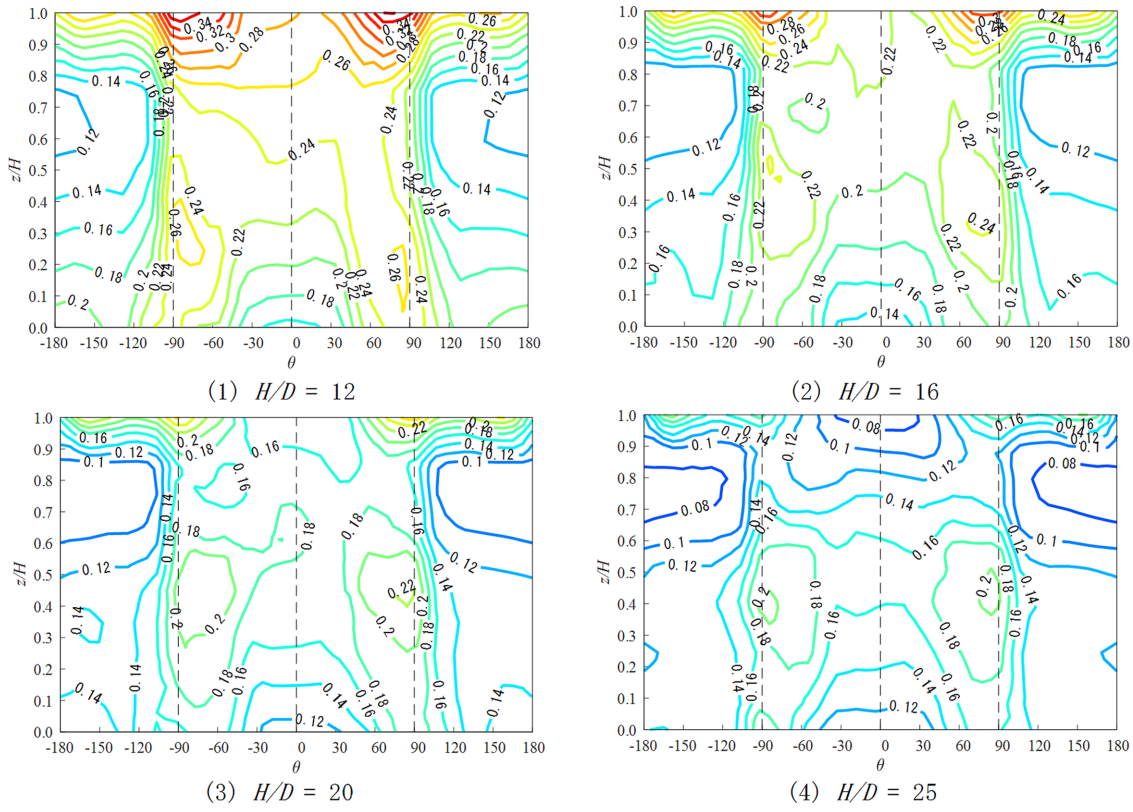


Figure 6. Comparison of fluctuating wind pressure coefficients with aspect ratio.

and cancel out the fluctuation of wake vortex.

Figure 7 compares the power spectrum density of C_p' with aspect ratio. A narrow band of spectral peaks is seen at normalized frequency $fD/U_H = 0.06$~0.09. These peaks were examined by comparing them with the results of experiments in which the wind speed was changed, but their clear cause is unknown. They tend to exist at a constant level even at low wind speeds and is presumed to be unrelated to the flow field. However, clarification of this phenomenon is beyond the scope of this paper. In the figure, at $\theta = 0^o$, the magnitude of the fluctuating wind pressure spectrum is affected by the turbulence intensity of the approaching flow. At $\theta = 90^o$, the spectral peak due to the Karman vortex is seen at $fD/U_H = 0.15$~0.20, and the magnitude is almost the same regardless of aspect ratio. At $\theta = 162^o$, a spectral peak due to the Karman vortex is seen as well. However, at $z/H = 0.90$~0.95, there is spectral peak at $fD/U_H = 0.05$ for only $H/D = 25$. This is thought to be due to end-cell-induced vibration according to Kitagawa et al. (2001). It does not clarify why this spectral peak does not appear for other than $H/D = 25$, but it may be related to the vortex shedding from the free edge becoming localized as the aspect ratio increases, as shown in Figure 5.

4. Proper Orthogonal Decomposition

The POD technique has been used in many fields, and it was performed to investigate the organizational structure of the fluctuating wind pressure acting on the building by many researchers (e.g., Bienkiewicz et al., 1995; Kikuchi et al., 1997; Tamura et al., 1999). Figure 8 shows typical POD modes of fluctuating wind pressure coefficient C_p' of $H/D = 25$ model. C_p' can be classified into symmetrical or asymmetrical modes. Furthermore, the POD mode can be seen only at the free end in the 13th mode, but this has only been seen for $H/D = 25$. Figure 9 shows the contribution rates and cumulative contribution rates for POD modes up to the 30th mode. The contributions of the individual modes are 24% for the 1st mode, 9% for the 2nd mode, and 8% for the 3rd mode. A contribution for the 13th mode is found only for $H/D = 25$ and its 2%. The cumulative contribution is 80% of the total wind pressure for the 16th modes, and 92% for the 30th modes.

Figure 10 shows the fluctuating wind pressure distribution synthesized only for symmetric or only for asymmetric modes from POD modes up to the 30th order. Figure 11 shows the fluctuating wind force spectrum calculated by synthesized fluctuating wind pressure. In the figure also shows the fluctuating wind force spectrum calculated by wind pressure experiments result as a comparison. The results of the wind force spectrum of the symmetric modes approximately reproduce the fluctuating drag force spectrum (see Figure 11(1)). On the other hand, the results of the wind force spectrum of the asymmetric modes approximately reproduce the fluctuating lift force spectrum (see Figure

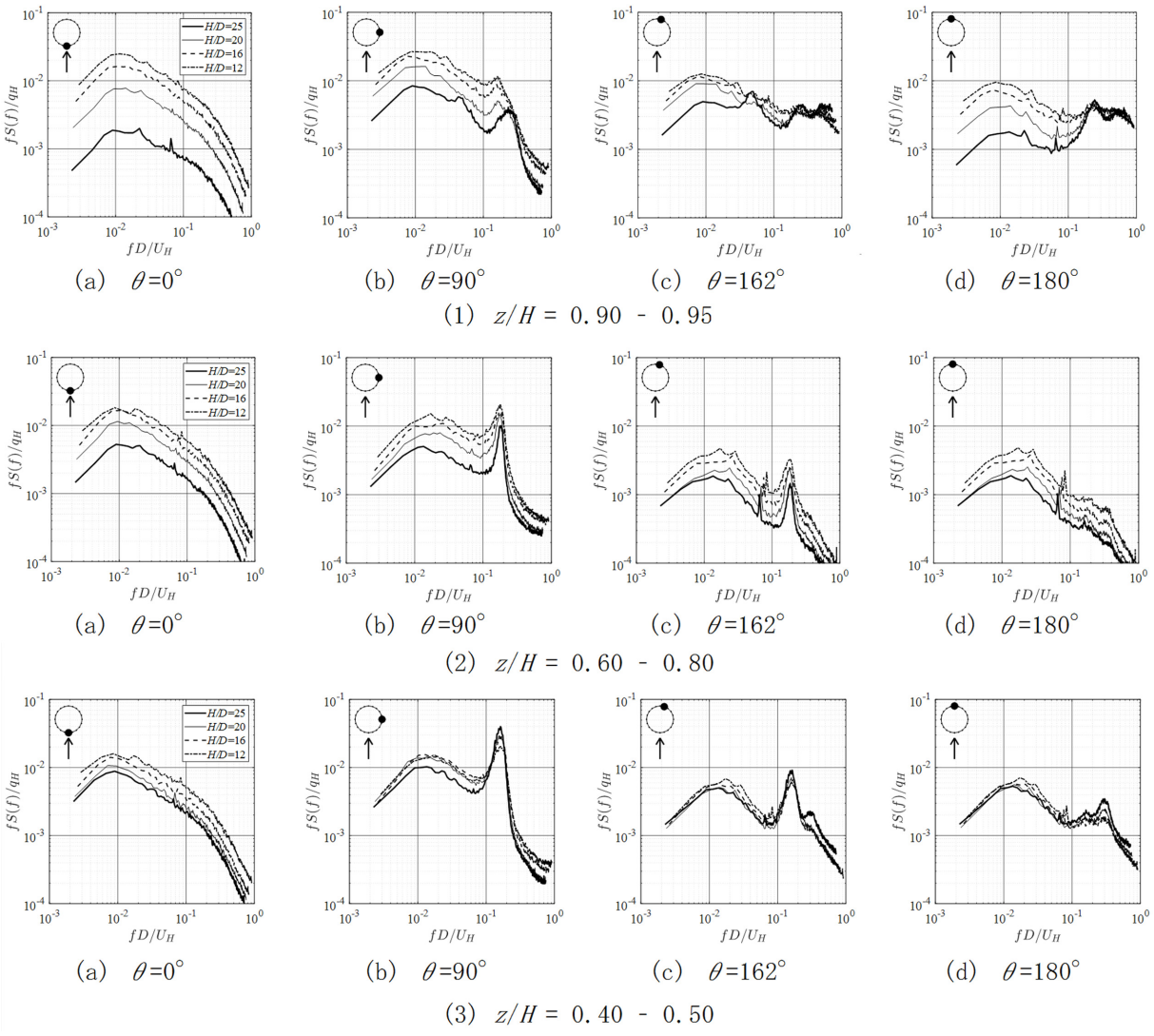


Figure 7. Power spectrum density of fluctuating wind pressure coefficient.

11(2)). In follow section, discussion is focused on the procedure of estimation the fluctuating wind force spectrum.

5. Fluctuating Lift Force Supectrum

As shown in the previous sections, the fluctuating wind pressures acting on the circular cylinder are symmetrical, in particular, the symmetric modal component is the fluctuating drag force and the asymmetric modal component is the fluctuating lift force. Therefore, in this study, the fluctuating wind force of the circular cylinder is considered to be divided to for the left and right sides, and then their fluctuating wind force spectrum is discussed. Figure 12 shows the definition of the wind force when the circular cylinder is divided into left and right sides.

Figure 13 shows the power spectrum density of the fluctuating lift force of the one-side-cylinder F_{yL} and F_{yR}. By comparing F_{yR} and F_{yL}, it can be seen that the power spectrum shapes are almost the same because the left and right side cylinders are symmetrical, and the spectral peak of the Strouhal component can be confirmed at around $fD/U_H = 0.16$. By comparing F_{yR}, F_{yL} and Fy, it can be seen that the spectral peaks coincide at around $fD/U_H = 0.16$, while spectral peaks are also observed at $fD/U_H = 0.06$ for F_{yR} and F_{yL}. As shown also in Figure 7, the clear cause of this is unknown.

However, clarification of this phenomenon is beyond the scope of this paper. On the other hand, it should be noted here that the low-frequency regions of F_{yR}, F_{yL} and F_x almost overlap. Although, the fluctuating drag and lift force spectrum of a circular cylinder have been proposed for each, Figure13 shows the possibility of predicting the fluctuating lift spectrum from the fluctuating drag spectrum if the correlation characteristics between the left and right fluctuating lift can be predicted. Therefore, the correlation characteristics of the left and right fluctuating lift forces were investigated.

Figure 14 shows the correlation characteristics of F_{yR}

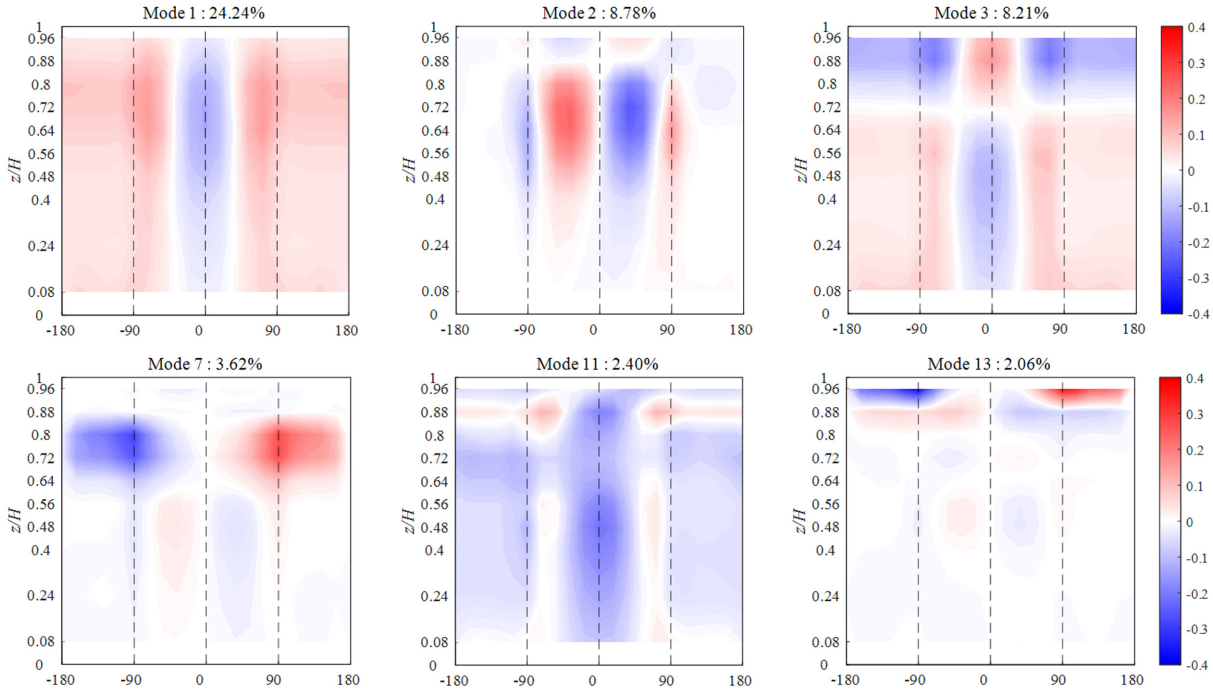


Figure 8. POD modes of fluctuating wind pressure coefficient (*H/D*=25)

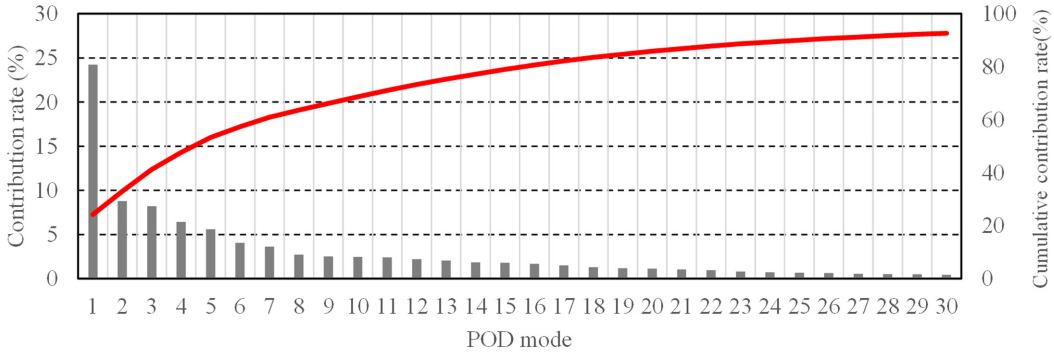


Figure 9. Contribution rate of POD mode.

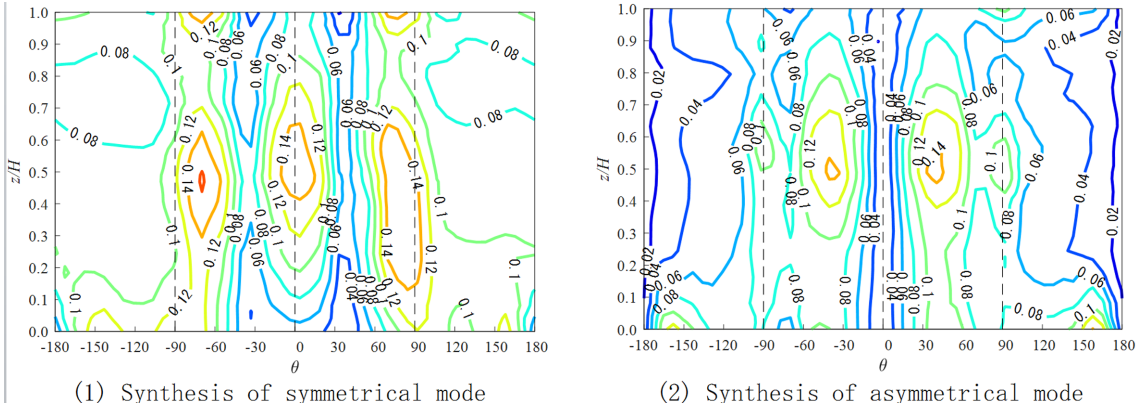


Figure 10. Comparison of fluctuating wind pressure coefficient by Synthesis of POD mode.

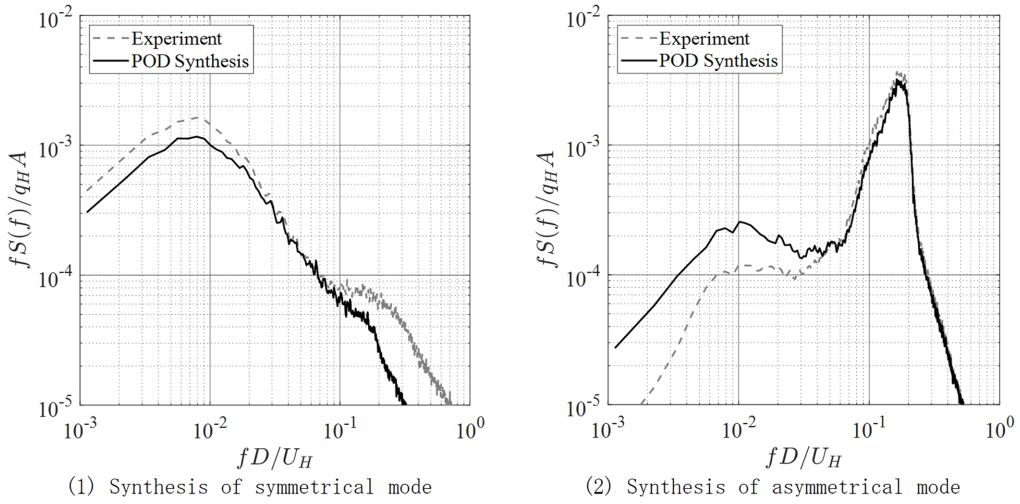


Figure 11. Comparison of power spectrum density by synthesis of POD mode.

and F_{yL}. The Co-coherence C_{LR} changes from -1 to 1 as fD/U_H changes from 0 to 0.1, and C_{LR} gradually approaches 0 as $fD/U_H > 0.2$. On the other hand, the phase angle is($\phi = \pi$ or $-\pi$ for $fD/U_H < 0.07$ and($\phi = 0$ for $fD/U_H > 0.07$. In the range of $fD/U_H < 0.07$, the left and right fluctuating lift forces are in opposite phase and cancel each other, but in

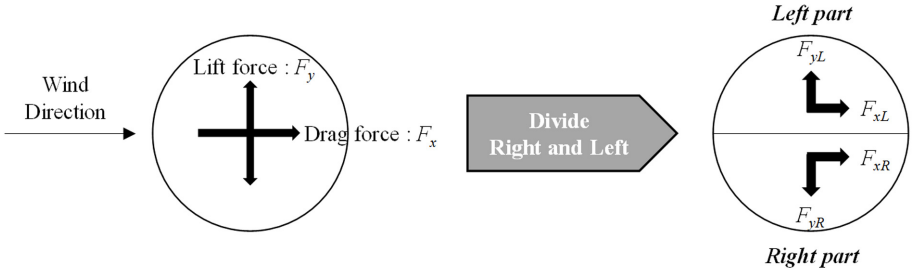


Figure 12. Definition of wind force in the one-side-cylinder.

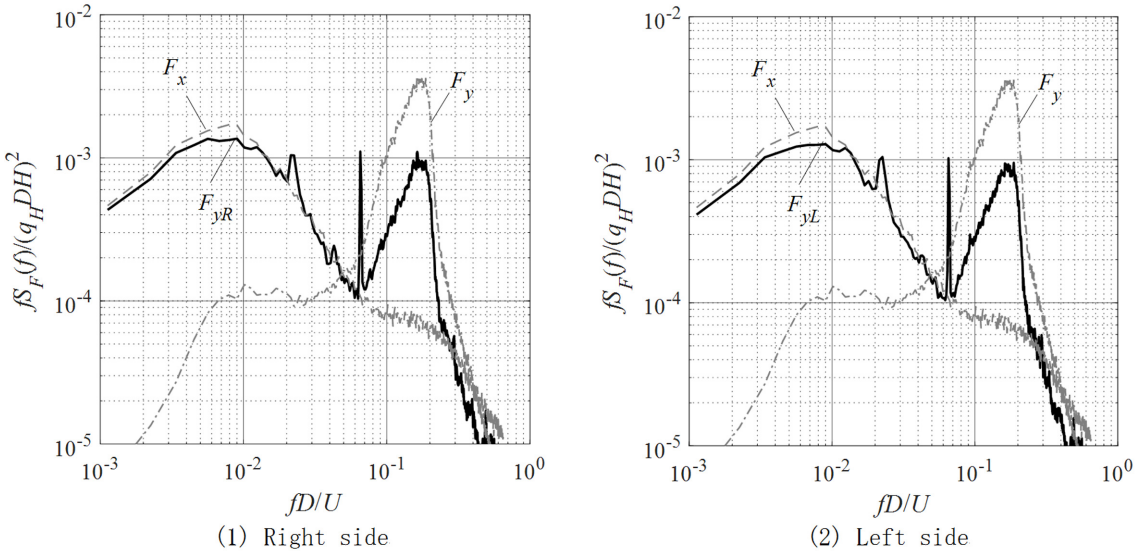


Figure 13. Power spectrum density of fluctuating lift force of one-side-cylinder.

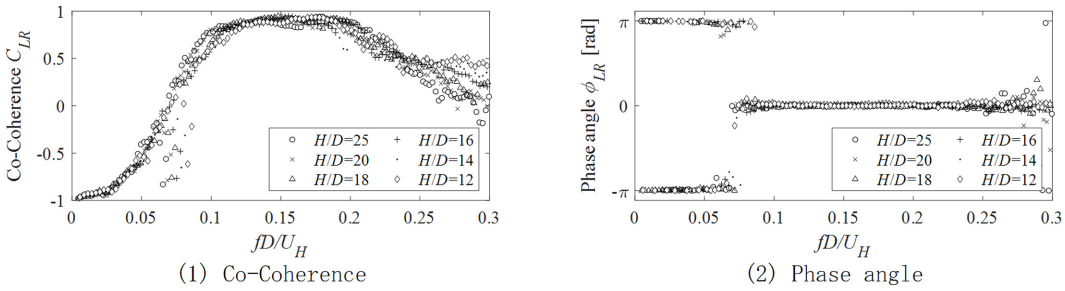


Figure 14. Correlation characteristics of F_{yR} and F_{yL}.

the range of $0.07 < fD/U_H < 0.2$, they are in phase and only the fluctuating lift due to the Karman vortex is enhanced. For $fD/U_H > 0.2$, C_{LR} approaches 0 and $(\phi$ approaches 0, and the effect on the fluctuating lift force becomes small. Also, C_{LR} and ϕ show the same tendency regardless of aspect ratio H/D.

Based on these results, in this study suggest a procedure for estimating the fluctuating lift force spectrum in the following two steps. Firstly, estimate the fluctuating lift force spectrum of a one-side-cylinder using the fluctuating drag force spectrum and Karman vortex component. Secondly, combine the fluctuating lift force spectrum of one-side-cylinder using the correlation characteristics shown in Figure 14. These procedures are expressed in the following equation. First of all, the fluctuating drag spectrum of a circular cylinder is assumed to be given by equation (3).

$$S_{Fx}(f) = 4\left(q_H I_H C_D DH\right)^2 \left|\chi_{UF}(f)\right|^2 \frac{S_U(f)}{{\sigma_U}^2} \tag{3}$$

where q_H is velocity pressure at top, I_H is turbulence intensity at top, C_D is drag coefficient, D is structure width, and H is structure height. The aerodynamic admittance $|X_{UF}(f)|^2$ is assumed to be given by equation (4) (Vickery, B. J., 1968).

$$\left|\chi_{UF}(f)\right|^2 = \frac{1}{1+\left(\frac{2f\sqrt{A}}{U_H}\right)^{4/3}} \tag{4}$$

The power spectrum of the fluctuating wind speed is assumed to be represented by a Karman-type spectrum and is given by equation (5).

$$\frac{S_U(f)}{{\sigma_U}^2} = \frac{4L(Z)/U(Z)}{\left[1+70.78\{fL(Z)/U(Z)\}^2\right]^{5/6}} \tag{5}$$

The fluctuating lift spectrum of the one-side-cylinder $S_{FyL(R)}$ is obtained by adding the power spectrum of the Karman vortex component to the fluctuating drag spectrum S_{Fx} shown as Figure 13, and is given by equation (6).

$$S_{FyL(R)}(f) = k \cdot S_{Fx}(f) + \lambda(f) \tag{6}$$

where k is a constant that expresses the degree of agreement between the gust components of $S_{FyL(R)}$ and S_{Fx}. In this study, $k = 1$ is used because the gust components of $S_{FyL(R)}$ and S_{Fx} are almost the same as shown in Figure 13. λ is the Karman vortex component of the fluctuating lift spectrum of the one-side-cylinder, and is obtained from equation (6) by the difference between $S_{FyL(R)}$ and S_{Fx}.

Figure 15 shows the results of λ. The normalized frequency $fD/U_H < 0.1$ is considered to be mainly due to the gust component. Although λ can be negative, the figure shows only the positive range in order to focus on the fluctuating lift force by the Karman vortex. It can be seen that A increases as the aspect ratio increases. According to Schewe (1983), the fluctuating lift amplitude of a circular cylinder in the subcritical or transcritical region of the Reynolds number is a Gaussian distribution. Therefore, λ is given by a deformed form of the Gaussian distribution by equation (7).

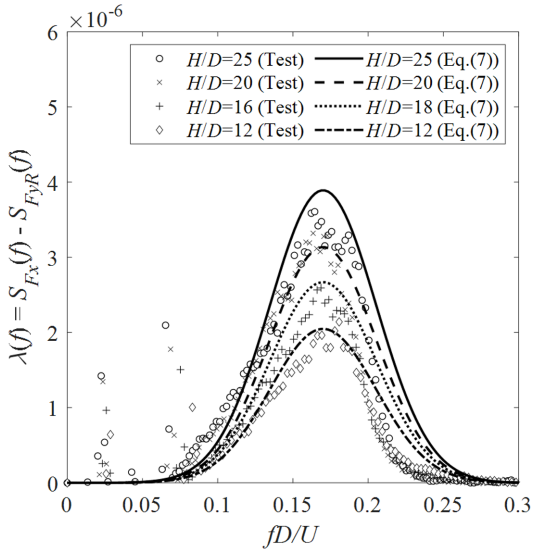


Figure 15. Power spectrum difference λ of S_{Fx} and S_{FyR}.

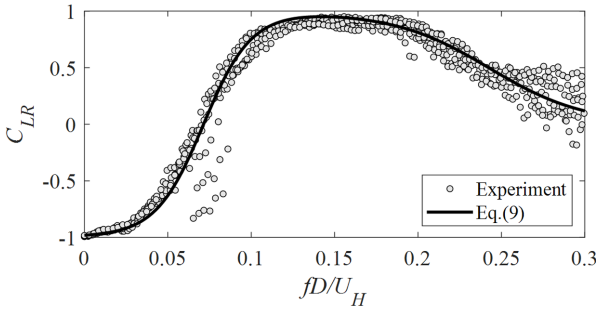


Figure 16. Comparison of Co-coherence and suggested model.

$$\lambda(f) = 5.0\times10^{-6}\left(\frac{H}{12D}\right)^2 \exp\left\{-\left(\frac{f^* - 0.16}{0.05}\right)^2\right\} \quad (7)$$

Figure 15 also shows the approximate results using equation (7), which are coincident with the experimental results.

Finally, the cross spectrum is calculated using the coherence C_{LR}, and the fluctuating lift spectrum S_{Fy} is obtained from equation (8).

$$S_{Fy}(f) = S_{FyL}(f) + S_{FyR}(f) + 2\sqrt{S_{FyL}(f)S_{FyR}(f)}C_{LR}(f) \quad (8)$$

The coherence C_{LR} has different properties in different frequency bands, as shown in Figure 14, and cannot be expressed in terms of a general exponential variation.

On the other hand, there is no effect of aspect ratio, and C_{LR} is expressed by a multiplication of the sigmoid function. The suggested equation is equation (9).

Table 1. Parameters for validation of suggestion

Component	Symbol	Unit	$H/D = 25$
Wind speed	U_H	m/s	17.34
Turbulence Intensity	I_H	%	6.0
Turbulence length scale	L_H		1/160
Drag force coefficient	C_D		0.56

$$C_{LR}(f^*) = \left(\frac{\exp(\alpha\cdot f^*) - \exp(\varepsilon)}{\exp(\beta\cdot f^*) + \exp(\varepsilon)}\right)\left(-\frac{\exp\left(\gamma\left(f^* - 0.07\right)\right) - \exp(\kappa)}{\exp\left(\delta\left(f^* - 0.07\right)\right) + \exp(\kappa)}\right) \quad (9)$$

where, $f^* = fD/U_H$ and each coefficient is a constant: $\pi = 70$, $\gamma = 20$, $\delta = 35$, $\varepsilon = 5$, $\kappa = 5.5$. Figure 16 compares experimental and equation (8) results. The suggested equation is able to express the variation of coherence with frequency.

Figure 17 compares the fluctuating drag coefficient spectrum and fluctuating lift coefficient spectrum calculated based on these suggested equations with wind pressure experimental results. Table 1 shows the parameters used in the calculations. The turbulence scale L_H was calculated using equation (10) because the surface of the model is provided with roughness.

$$L_H = 100\times\left(\frac{H}{30}\right)^{0.5}\times\eta \quad (10)$$

where η is the model scale (=1/160). In Figure 17, although the experimental values of the fluctuating drag spectrum exceed the suggested equation results in the low-frequency range, the trend is generally captured. The experimental results also exceed the proposed formula results in the range of dimensionless frequencies $fD/U_H >$ 0.1. However, the drag force of the cylinder is obtained

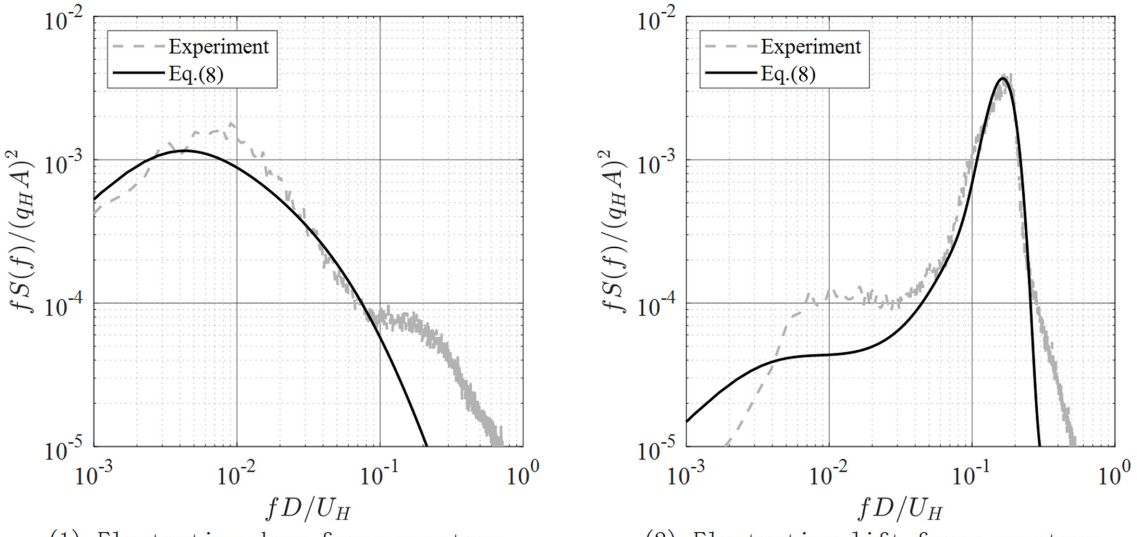


Figure 17. Comparison of power spectrum density with suggested model.

by multiplying the wind pressure data at each measurement point by the wind load area and normal vector. It is possible that the Karman vortex component has effect on the fluctuating drag force.

Alternatively, the roughness is also imparted on the cylinder surface, which may have caused localized vortices.

The fluctuating lift spectrum is generally consistent with the experimental values for the Karman vortex component (see Figure 17(2)). However, in the range of fD/U_H<0.03 or fD/U_H>0.3, there is a difference between the suggested equation results and the experimental values. Their influence is small because the fluctuating lift coefficient, which is calculated by integrating the fluctuating lift spectrum in Figure 17(2), is in general agreement with the experimental value. In this case, the experimental value of the fluctuating lift coefficient C_L' = 0.049, but C_L' calculated by integrating the fluctuating lift spectrum in Figure 17(2) using the trapezoidal method is 0.048.

6. Conclusion

In this study, wind pressure experiments were carried out using high aspect ratio circular cylinder, and considered about organizational structure of fluctuating wind pressure distribution applied POD technique. As a result, the knowledge were obtained as follows.

1) As the aspect ratio increases, the two-dimensionality of the vortex shedding from the cylinder surface increases.

2) As the aspect ratio increases, the three-dimensionality of the vortex shedding generated at the free end of the cylinder becomes more localized, and at an aspect ratio of 25, a more developed vortex than the Karman vortex is observed.

3) The organizational structure of the fluctuating wind pressure can be divided into symmetrical or asymmetrical.

4) The fluctuating wind pressure due to the vortex shedding generated at the free end, which is only appears as a characteristic fluctuating wind pressure mode for an aspect ratio of 25.

In addition, based on these results, a method for evaluating the fluctuating wind power spectrum was also discussed. The validity of this suggested method will be verified by calculating the response in the future. However, this suggestion is not sufficient for vortex-induced vibrations, which are often a problem for cylindrical structures. Because it is necessary to properly evaluate aerodynamic negative damping effects and other factors. In such cases, it is desirable to conduct an evaluation using the wake oscillator model proposed by Tamura and Amano (1984), for example. On the other hand, recently, to ensure resilience against large earthquakes, consideration has been given to vibration control devices to tower-supported chimneys. If the additional damping is large and vortex-induced vibration is not a problem, the suggested method may useful to evaluate the response of forced vibration.

References

Architectural Institute of Japan. (2015). AIJ Recommendations for Loads on Buildings. Maruzen, (in Japanese)

Bienkiewicz, B., Tamura, Y., Ham, H-J., Ueda, H., Hibi, K. (1995). "Proper orthogonal decomposition and reconstruction of multi-channel roof pressure. J. Wind Eng. Ind. Aerodyn., Vols 54-55, 369-381

Davenport, A. G. (1967). "Gust Loading Factors. J. Struct. Div., ST3, 11-34.

Homma, M., Maeda, J., Susuki, T., Makihata, T. (2003). "Wind Response of a Tower Supported Steel Stack. J. Tech. Design, No.17, 97-101, (in Japanese).

Katagiri, J., Marukawa, H., Nakamura, O., Tamura, Y., Ookuma, T. (1986). "The Characteristics of Aerodynamic Forces Acting on Cantilevered Circular Cylinders. Proc., 9th National Symposium on Wind Eng., JAWE, Tokyo, 103-108, (in Japanese).

Kikuchi, H., Tamura, Y., Ueda, H., Hibi, K. (1997). "Dynamic Wind Pressures Acting on a Tall Building Model - Proper Orthogonal Decomposition. J. Wind Eng. Ind. Aerodyn., Vols. 69-71, 631-646.

Kitagawa, T., Fujino, Y., Kimura, K., Mizuno, Y. (2001). "Wind Pressure on End-Cell-Induced Vibration of Circular Cylinder. J. Eng. Mech., 127(11), 1135-1143.

Marukawa, H., Tamura, Y., Sanada, S., Nakamura, O. (1984). "Lift and Across - Wind Response of a 200m Concrete Chimney. J. of Wind Eng., No.19, 37-52, (in Japanese).

Roshko, A. (1961). "Experiments on the Flow Past a Circular Cylinder at Very High Reynolds Number. J. Fluid Mech. 10(3), 345-356.

Schewe, B. (1983). "On The Force Fluctuations Acting on a Circular Cylinder in Crossflow from Subcritical up to Transcritical Reynolds Number. J. Fluid Mech. 133, 265-285.

Tamura, Y., Amano, A. (1984). "Vortex Induced Vibration of Circular Cylinder: part III Model of Vortex Induced Oscillations of Continuous System. Transactions of the AIJ, 337, 65-72, (in Japanese with English summary)

Tamura, Y., Suganuma, S., Kikuchi, H., Hibi, K. (1999). "Proper Orthogonal Decomposition of Random Wind Pressure Field. J. Fluids. Struct., 13, 1069-1095.

Vickery, B. J. (1968). "Load Fluctuations in Turbulent Flow. J. Eng. Mech. Div., EM1, 31-46.

Vickery, B. J., Clark, A. W. (1972). "Lift or Across-Wind Response of Tapered Stacks. J. Struct. Div., ST1, 1-20.